

Dopant-Free Hole Transporting Molecules for Highly Efficient Perovskite Photovoltaic with Strong Interfacial Interaction

Fanxu Meng, Yu Jia, Jiantao Wang, Xiaoyu Huang, Zhigang Gui, Li Huang, Ruxue Li, Rui Chen, Jing Xu, Wei Chen, Zhubing He, Hsien-Yi Hsu, Enwei Zhu,* Guangbo Che,* and Hsing-Lin Wang*

One of the attractive ways to develop efficient and cost-effective inverted perovskite solar cells (PVSCs) is through the use of dopant-free hole transporting materials (HTMs) with facile synthesis and a lower price tag. Herein, two organic small molecules with a fluorene core are presented as dopant-free HTMs in inverted PVSCs, namely, FB-OMeTPA and FT-OMeTPA. The two molecules are designed in such a way they differ by replacing one of the benzene rings (FB-OMeTPA) with thiophene (FT-OMeTPA), which leads to a significantly improved coplanarity as manifested in the redshift of the absorbance and a smaller bandgap energy. Density functional theory calculations show that FT-OMeTPA has a strong Pb^{2+} -S interaction at the FT-OMeTPA/perovskite interface, allowing surface passivation and facilitating charge transfer across interfaces. As a result, the PVSCs based on FT-OMeTPA exhibit a much higher hole mobility, power conversion efficiency, operational stability, and less hysteresis as compared with devices based on FB-OMeTPA.

to the inorganic silicon solar cells, hybrid PVSCs are lightweighted, processible at low temperature, and have tunable electronic and optical properties.^[3,4] Worth noting that high PCE over 20% can usually be achieved by the normal (n-i-p) configuration via inserting a hole transporting layer (HTL) between perovskite and metal electrode.^[2,5-9] The most popular HTL in this configuration is 2,2',7,7'-tetrakis (N,N-di-methoxyphenyl-amine) 9,9-spirofluorene (Spiro-OMeTAD); however, Spiro-OMeTAD requires additional chemical doping and oxidation process to achieve better conductivity and energy level match, leading to a complicate fabrication process.^[10-12] Besides, the hydrophilic dopants can bring in the degradation issues, which have negative impacts on the stability of PVSCs.^[13-15] Therefore, much effort has

been devoted to develop dopant-free hole transporting materials (HTMs) applied in either normal or inverted (p-i-n) PVSCs (e.g., transparent conductive substrate/HTL/perovskite/electron

It is exciting that the power conversion efficiency (PCE) of hybrid organic-inorganic halide perovskite solar cells (PVSCs) has grown from 3.8%^[1] to 25.2%^[2] in the last decade. In contrast

Dr. F. Meng, J. Wang, J. Xu, W. Chen, Prof. Z. He, Prof. H.-L. Wang
Department of Material Science and Engineering
Southern University of Science and Technology
Shenzhen, Guangdong 518055, P. R. China
E-mail: wangxl3@sustc.edu.cn

Dr. Z. Gui
SUSTech Academy for Advanced Interdisciplinary Studies
Department of Physics
Southern University of Science and Technology
Shenzhen, Guangdong 518055, P. R. China


Prof. L. Huang
Department of Physics
Southern University of Science and Technology
Shenzhen, Guangdong 518055, P. R. China

R. Li, Prof. R. Chen
Department of Electrical and Electronic Engineering
Southern University of Science and Technology
Shenzhen, Guangdong 518055, P. R. China

Y. Jia, Prof. G. Che
Key Laboratory of Preparation and Application of Environmental Friendly Materials
Jilin Normal University
Ministry of Education
Changchun 130103, P. R. China
E-mail: guangboche@jlnu.edu.cn

Prof. E. Zhu
College of Chemistry
Jilin Normal University
Siping 136000, P. R. China
E-mail: zhuenwei@jlnu.edu.cn, zhuenwei05@126.com

X. Huang, Prof. H.-Y. Hsu
School of Energy and Environment
City University of Hong Kong
Kowloon Tong, Hong Kong 999007, P. R. China

 The ORCID identification number(s) for the author(s) of this article can be found under <https://doi.org/10.1002/solr.201900319>.

DOI: 10.1002/solr.201900319

transporting layer (ETL)/metal electrode) for their simple fabrication process, high PCE over 18%, and low hysteresis.^[16–19]

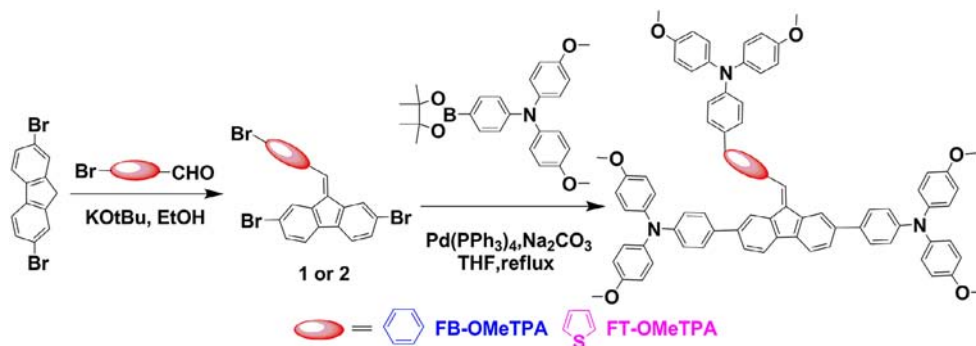
The HTL plays a critical role in inverted PVSCs than that in the normal configuration. In the inverted structure, HTL not only plays the role of extracting the holes and block the electrons from perovskite, but also facilitating the formation of perovskite films with high crystalline quality. Inorganic p-type HTLs, such as NiO_x, have been used in efficient and stable inverted PVSCs;^[20–22] however, a high-temperature annealing step is usually needed. Polymer HTL, poly(3,4-ethylenedioxythiophene):poly(styrenesulfonate) (PEDOT:PSS), is very popular in both polymer solar cells and PVSCs, but it still suffers from its hydrophilic nature and energy level mismatch issues.^[23,24] Another hydrophobic polymer, poly(bis(4-phenyl)(2,4,6-trimethylphenyl)amine) (PTAA), is favored for the reported efficiency over 20% of dopant-free p-i-n devices,^[16] but its high cost is not desirable for the commercial production of PVSCs. Comparing with the inorganic and polymer semiconductor HTLs, small organic molecule is an alternative for constructing dopant-free inverted PVSCs, mainly due to the ease of the synthesis and purification, tunable interfacial interaction, and optoelectronic properties.^[25,26]

Herein, the central cores based on fluorene-bridge-benzene unit (FB) and fluorene-bridge-thiophene unit (FT) were coupled with triarylamine groups (TPA), a kind of popular functional group for efficient hole transport in PVSCs.^[17,19,27] Our HTMs, namely, FB-OMeTPA and FT-OMeTPA, require only two step synthesis; therefore, the design synthesis is facile and low cost compared with most of the HTM molecules. Comparing with FT-OMeTPA, FB-OMeTPA has a slightly deeper highest occupied molecular orbital (HOMO), whereas FT-OMeTPA exhibits a much higher hole mobility by introducing thiophene unit. In addition, the incorporation of the thiophene unit into FT-OMeTPA is beneficially considered for the defect passivation between HTMs and perovskite interface via the Pb²⁺–S interaction.^[28,29] The optimized PCE of inverted PVSCs based on FT-OMeTPA is 17.57%, which is higher than that of the device based on FB-OMeTPA (14.35%). The inverted PVSCs based on FT-OMeTPA also show a smaller hysteresis. Our results show that the newly synthesized HTMs are promising candidates for highly efficient, low-cost PVSCs.

The synthetic routes of FB-OMeTPA and FT-OMeTPA are shown in **Scheme 1**, and detailed synthetic procedures are listed in Supporting Information. Our facile synthesis only requires two-step reaction with low complexity. First, 2,7 dibromofluorene

was condensed with 4-bromobenzaldehyde and 5-bromothiophene-2-carbaldehyde through the Knoevenagel reaction to yield key intermediates **1** and **2**, respectively. Subsequently, intermediates **1** and **2** were coupled with 4-methoxy-N-(4-methylthiophenyl)-N-(4-(4,4,5,5-tetramethyl-1,3,2-dioxaborolan-2-yl)phenyl)aniline via a Pd-catalyzed Suzuki reaction to give FB-OMeTPA and FT-OMeTPA, respectively. The as-synthesized compounds for PVSCs were purified through simple column chromatography and recrystallization to avoid the expensive sublimation process. The chemical structures of FB-OMeTPA and FT-OMeTPA were carefully characterized by means of nuclear magnetic resonance spectroscopy (NMR) (Figure S1–S8, Supporting Information) and matrix-assisted laser desorption ionization-time of flight (MALDI-TOF) mass spectrometry (Figure S9 and S10, Supporting Information). Both compounds exhibit good solubility in common organic solvents, such as chloroform, toluene, and chlorobenzene, but there is a higher solubility (<10 mg mL⁻¹) of FB-OMeTPA than that (<3 mg mL⁻¹) of FT-OMeTPA in highly polar solvents, such as dimethyl sulfoxide (DMSO). Therefore, FT-OMeTPA shows a better tolerance to perovskite precursor solutions than FB-OMeTPA. The cost for laboratory synthesis and purification of both FB-OMeTPA (\$26/g) and FT-OMeTPA (\$28/g) is much lower than that of spiro-OMeTAD (see cost calculation in Supporting Information).

The thermal properties of FB-OMeTPA and FT-OMeTPA were measured by thermogravimetric analysis (TGA) and differential scanning calorimetry (DSC) scans (**Figure 1a,b**). The TGA curves of both compounds show good thermal stability, and the decomposition temperatures (*T_d*) at the 5% weight loss are 427 °C for FB-OMeTPA and 426 °C for FT-OMeTPA. DSC results reveal glass transition temperature (*T_g*) for FB-OMeTPA and FT-OMeTPA at 120 and 113 °C, respectively. The results indicate that their amorphous nature may help to form uniform and pinhole-free HTL films.^[30,31] The normalized UV–Vis absorption spectrum of FB-OMeTPA and FT-OMeTPA in solid films is shown in **Figure 1c**. Both spectra feature two distinct absorption peaks. FB-OMeTPA exhibits absorption peaks at 380 and 450 nm with the absorption edge of 580 nm, whereas FT-OMeTPA exhibits absorption peaks of 360 and 490 nm with the absorption edge of 610 nm. The optical bandgap (*E_g*) of FB-OMeTPA and FT-OMeTPA is calculated to be 2.13 and 2.03 eV, respectively. Although such conjugated small molecules exhibit the absorption in the visible region, however, impact on device performance can be almost neglected as less than 10 nm



Scheme 1. The synthetic routes of FB-OMeTPA and FT-OMeTPA.

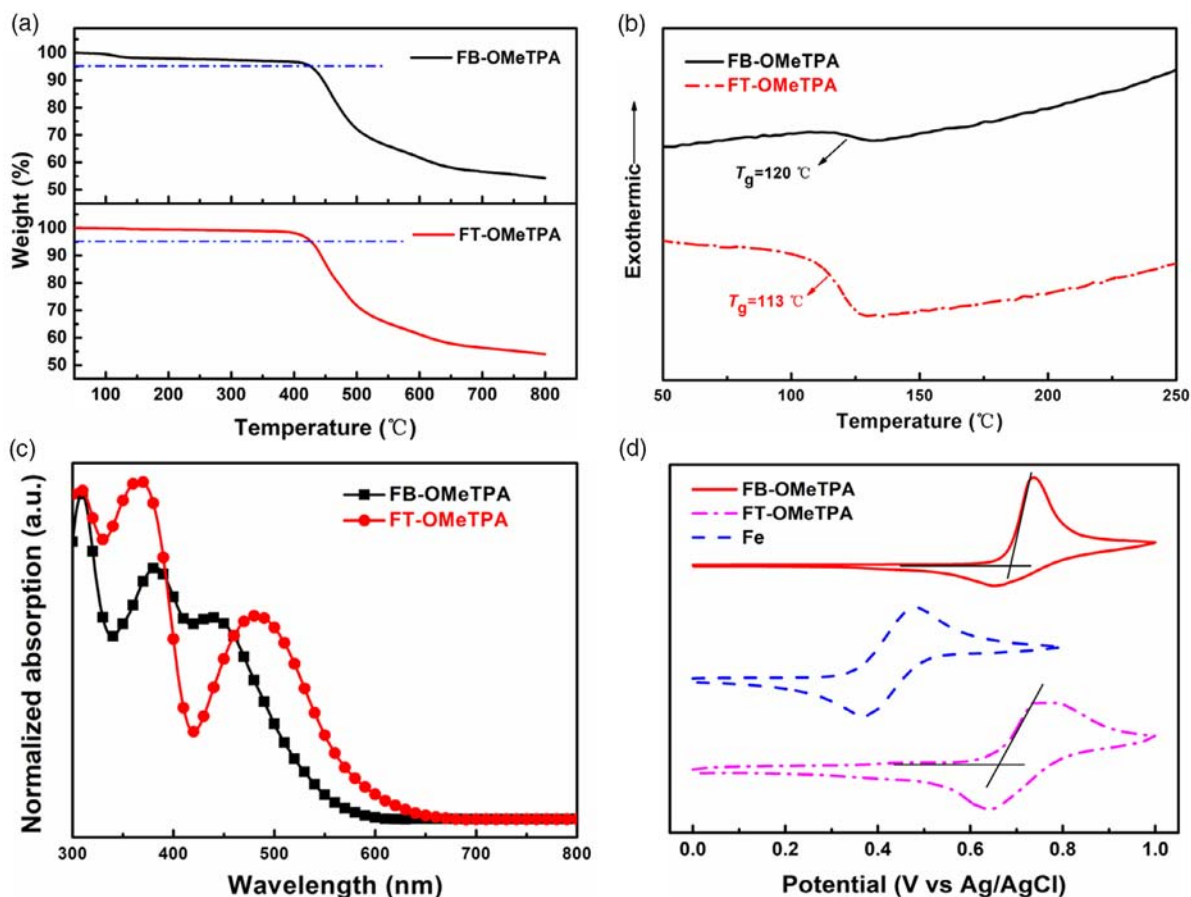


Figure 1. a) TGA and b) DSC curves of FB-OMeTPA and FT-OMeTPA. The heating rate was 10 °C min^{-1} . c) UV-Vis absorption spectra of FB-OMeTPA and FT-OMeTPA films. d) Cyclic voltammograms of FB-OMeTPA and FT-OMeTPA.

thick HTMs were deposited. As shown in the transmittance spectra (Figure S11, Supporting Information), there is only a decrease of no more than 10% in the range of 350–500 nm comparing with the transmittance of the bare indium tin oxide (ITO) glass substrate, ensuring that the majority of the incident photons can reach the perovskite active layer. Cyclic voltammetry (CV) measurements (Figure 1d) were carried out using ferrocene/ferrocenium (Fc/Fc⁺) as the internal standard to evaluate the energy levels of FB-OMeTPA and FT-OMeTPA. The CV curves of both compounds showed reversible oxidative peaks and no reduction peaks indicating the good electrochemical stability. The clear oxidation peaks are observed with an onset potential of 0.69 and 0.66 eV, respectively. Accordingly, the HOMO levels of FB-OMeTPA and FT-OMeTPA are estimated to be 5.14 and 5.11 eV, respectively.

Density functional theory (DFT) calculations at the B3LYP/6-31G* level were used to evaluate the HOMOs and the lowest unoccupied molecular orbitals (LUMOs) of the FB-OMeTPA and FT-OMeTPA (Figure 2). It is found that the HOMO molecular orbitals mainly localized on the fluorene-bridge-diarylamine moieties, whereas the LUMO molecular orbitals are mainly delocalized on the central fluorene-bridge-benzene moiety and fluorene-bridge-thiophene moiety of the two molecules. The coplanar feature resulting from replacing benzene ring with

thiophene unit is well manifested in the aforementioned electronic properties. It can be seen that the bridge-thiophene moiety with respect to the dibenzofulvene plane and bridge benzene of arylamine periphery groups in the FT-OMeTPA has the dihedral angles of 32.81 and 18.09°, respectively. Notably, the bridge-benzene moiety is evidently twisted to the dibenzofulvene plane and bridge benzene of arylamine periphery groups in the FB-OMeTPA with larger dihedral angles of 44.61 and 42.84°, respectively. As a result, the through space distance ($R_1 = 8.979$ Å) between the arylamine periphery groups and arylamine backbone groups in the FT-OMeTPA becomes longer compared with that ($R_1 = 4.403$ Å) of FB-OMeTPA (Figure 2), and the delocalization of the electron density through the thiophene bridge arylamine periphery group is observed in FT-OMeTPA due to the reduced steric hindrance, which can facilitate the redshifted absorption of spectra and the enhancement of hole mobility.

To investigate the performance of FB-OMeTPA and FT-OMeTPA in PVSCs, we fabricated the inverted PVSCs using FB-OMeTPA and FT-OMeTPA as the dopant-free HTLs, respectively. Briefly, FB-OMeTPA or FT-OMeTPA was spin-coated onto the ITO electrode and annealed at 150 °C to form a thin film with an approximate thickness of 10 nm. To demonstrate the morphology of these novel HTLs on ITO, measurement of atomic force microscopy (AFM) was carried out, as shown in

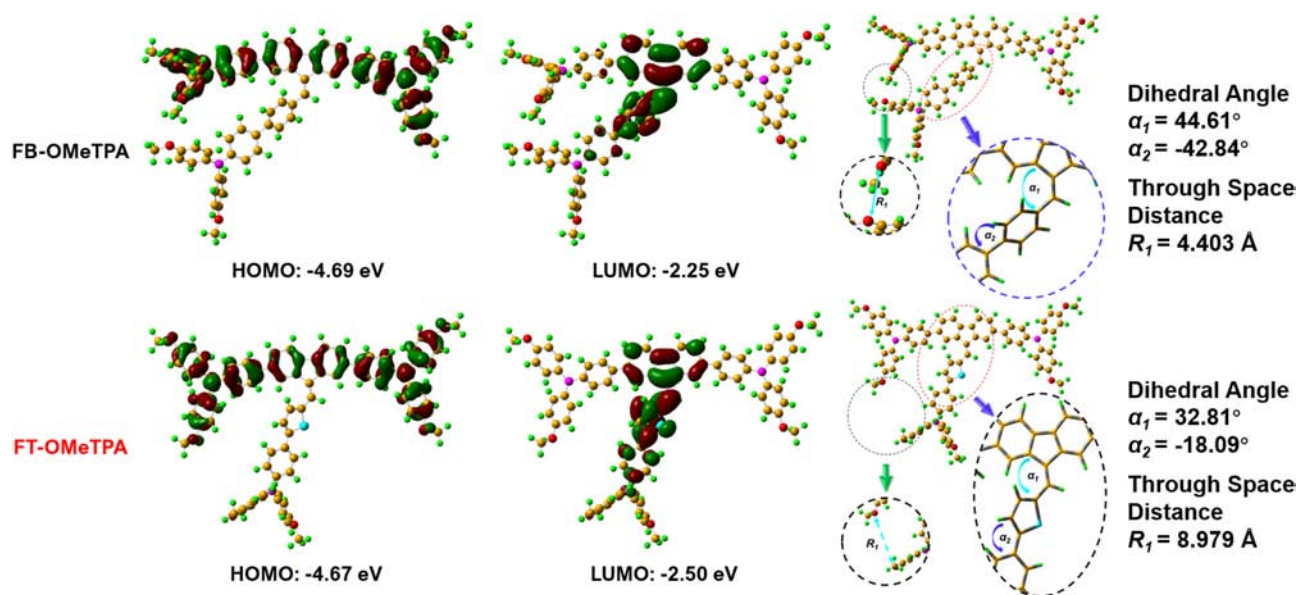


Figure 2. DFT-calculated HOMO and LUMO electronic structures, dihedral angles, and bond lengths of FB-OMeTPA and FT-OMeTPA.

Figure S12a,b, Supporting Information. The root mean square (RMS) is about 2.0 nm for FB-OMeTPA and 2.8 nm for FT-OMeTPA, respectively, indicating a smooth and uniform surface. In addition, the water contact angle is 80° for both two HTLs (Figure S12c,d, Supporting Information). The organic HTL with a relatively hydrophilic nature facilitates the formation of a high-quality perovskite film.^[28,32]

Then, the $(\text{CsPbI}_3)_{0.05}(\text{FAPbI}_3)_{0.83}(\text{MAPbBr}_3)_{0.17}{}_{0.95}$ (CsFAMA) mixed-perovskite layer was deposited onto the HTLs using a common antisolvent method as reported. The cross-sectional and top-view scanning electron microscopy (SEM) images of the CsFAMA perovskite films and devices (Figure 3) show that the perovskite layers on both two HTLs are about 590 nm thick and have almost the same distribution of grain size without any pin holes. The X-ray diffraction (XRD) data of CsFAMA perovskite films on HTLs are shown in Figure S13, Supporting Information, and the data are in accordance with the previously reported results,^[33] revealing a high crystallinity. Finally, [6,6]-phenyl-C61-butyric acid methyl ester (PCBM), bathocuproine (BCP), and Ag were deposited on the CsFAMA perovskite layer in sequence to form a complete PVSC (with the detailed information described in the Supporting Information).

The device architecture and energy alignment of materials are shown schematically in Figure 4a,b. FB-OMeTPA with a lower HOMO matches better with the valence band maximum (VBM) of CsFAMA perovskite than FT-OMeTPA. Figure 4c shows the current–voltage (J – V) characteristics of inverted PVSCs based on FB-OMeTPA and FT-OMeTPA as HTLs under 100 mW cm⁻² AM1.5G solar illumination with reverse scan (RS) and forward scan (FS). The device using FB-OMeTPA as HTL exhibits an open-circuit voltage (V_{OC}) of 1.11 V, a fill factor (FF) of 68.87%, and a short-circuit current density (J_{SC}) of 16.93 mA cm⁻², yielding a PCE of 12.9% at FS and 14.35% ($V_{\text{OC}} = 1.11$ V, FF = 76.75%, and $J_{\text{SC}} = 16.91$ mA cm⁻²) at RS, respectively. For the device based on FT-OMeTPA as HTL, we

observe a V_{OC} of 1.09 V for both FS and RS, which can be expected from the energy alignment and a significant improvement in PCE for FS (16.95%) and RS (17.57%) after optimization (Table S6 and S7, Supporting Information). The FT-OMeTPA-based device not only shows a higher PCE, but also displays a negligible hysteresis. The detailed results are summarized in Table 1. Moreover, the performances of the device based on FT-OMeTPA are very close to those of the reference devices based on dopant-free PTAA (Table S8, Supporting Information), suggesting that FT-OMeTPA is a promising HTM in PVSCs. The external quantum efficiency (EQE) spectra are shown in Figure 4d, and the EQE of the FT-OMeTPA-based devices is higher in the whole spectrum range than that of the devices with FB-OMeTPA as HTL. The integrated J_{SC} values estimated from the EQE spectra (16.37 mA cm⁻² for FB-OMeTPA, and 19.12 mA cm⁻² for FT-OMeTPA, respectively) are consistent with the J_{SC} values obtained from the J – V curves (Table 1). The corresponding stabilized PCE outputs (Figure 4e) of representative FB-OMeTPA- and FT-OMeTPA-based PVSCs are 12.67% and 16.12% under 100 mW cm⁻² AM1.5G solar illumination as a function of time at maximum power point, respectively. Moreover, the storage stability of the devices is also examined. The PVSCs were stored in the dark without any encapsulation for 120 h in ambient environment with 20% relative humidity (RH) at room temperature. As shown in Figure 4f, the FT-OMeTPA-based devices exhibit better long-term stability, retaining 96.3% of their initial efficiency after 120 h, comparing with FB-OMeTPA-based ones. One reason for the inferior device performance based on FB-OMeTPA might be the poor contact at the perovskite/FB-OMeTPA interface, resulting from the higher solubility of FB-OMeTPA in DMSO.

First-principles calculation has been performed based on DFT^[34,35] to better understand why FB-OMeTPA and FT-OMeTPA have a profound difference in device performances. Figure 5a shows the relaxed structures of FB-OMeTPA and

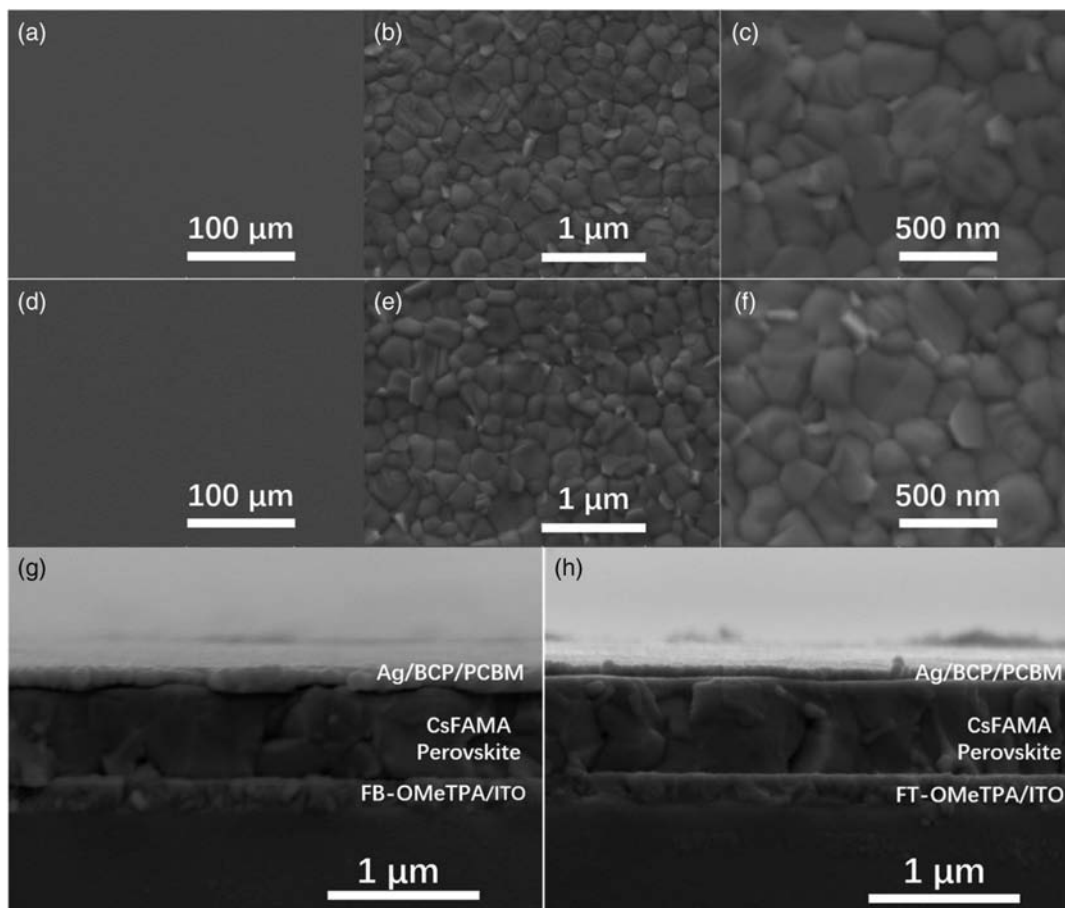


Figure 3. SEM top view of the CsFAMA perovskite film and cross-sectional image of the devices fabricated on a,b,c,g) FB-OMeTPA and d,e,f,h) FT-OMeTPA films as HTLs, respectively.

FT-OMeTPA molecules onto (001)-surfaces of the perovskite layers. Comparing the distances of the nearest pair of Pb–C and Pb–S in FB-OMeTPA and FT-OMeTPA absorption, it clearly shows a stronger interaction between FT-OMeTPA molecule and the perovskite layers (through Pb²⁺ and S atoms) than that between FB-OMeTPA and perovskite layers (through Pb²⁺ and C atoms). This is also reflected in the absorption energies of the two molecules mentioned earlier: 0.21 eV for FB-OMeTPA and 0.26 eV for FT-OMeTPA. Figure 5b,c gives the total and projected density of states (DOS) onto MAPbI₃ layers, FB-OMeTPA (panel b) and FT-OMeTPA (panel c). The valence bands from MAPbI₃ in both cases are mostly located below 0.5 eV. The HOMOs and LUMOs from the two types of OMeTPA molecules can be clearly identified in Figure 5b,c. The HOMOs are generally located between 0.4 and 0.0 eV, and the LUMOs are located above 2.2 eV, which suggests that both FB-OMeTPA and FT-OMeTPA can serve as good HTMs and are well consistent with previous reports.^[2,5–9,36] The gaps between LUMOs and HOMOs are also comparable with our aforementioned results. Figure 5d gives the position-resolved total electrostatic potentials along the *c* axis, which further proves that both FB-OMeTPA and FT-OMeTPA can indeed function as HTMs in our solar cells.

However, there are two apparent differences between them from the projected DOS. First, the HOMO from FB-OMeTPA

overlaps with the next molecular orbital just below it (HOMO-1), whereas the HOMO from FT-OMeTPA keeps a small gap from the HOMO-1. Second, the HOMO-1 from FT-OMeTPA overlaps closely with the top of valence bands from the perovskite layers (likely due to the stronger interaction between FT-OMeTPA molecule and the MAPbI₃ surface), which is believed to help the transport of generated holes to the HTM through the interface after light absorption. This is consistent with our experimental measurements that there is higher hole mobility observed in our solar cells using FT-OMeTPA than using FB-OMeTPA as HTM (Figure S13, Supporting Information). Figure 5e gives the charge density difference between the whole system (MAPbI₃ layers with FB/FT-OMeTPA absorbed) and the sum of individual constituents (MAPbI₃ layers and FB/FT-OMeTPA molecule). The charge redistribution is more significant in FT-OMeTPA case, which corroborates with our arguments mentioned earlier that stronger interaction exists between FT-OMeTPA and perovskite surface and facilitates the hole transport from the perovskite layers to the HTM.

X-ray photoelectron spectroscopy (XPS) measurements are performed to find the direct evidence of Pb²⁺–S interactions between perovskites and FT-OMeTPA, which is shown in Figure S14, Supporting Information. By introducing a thin layer of FT-OMeTPA on the perovskite film, a left shift of 0.8 eV at

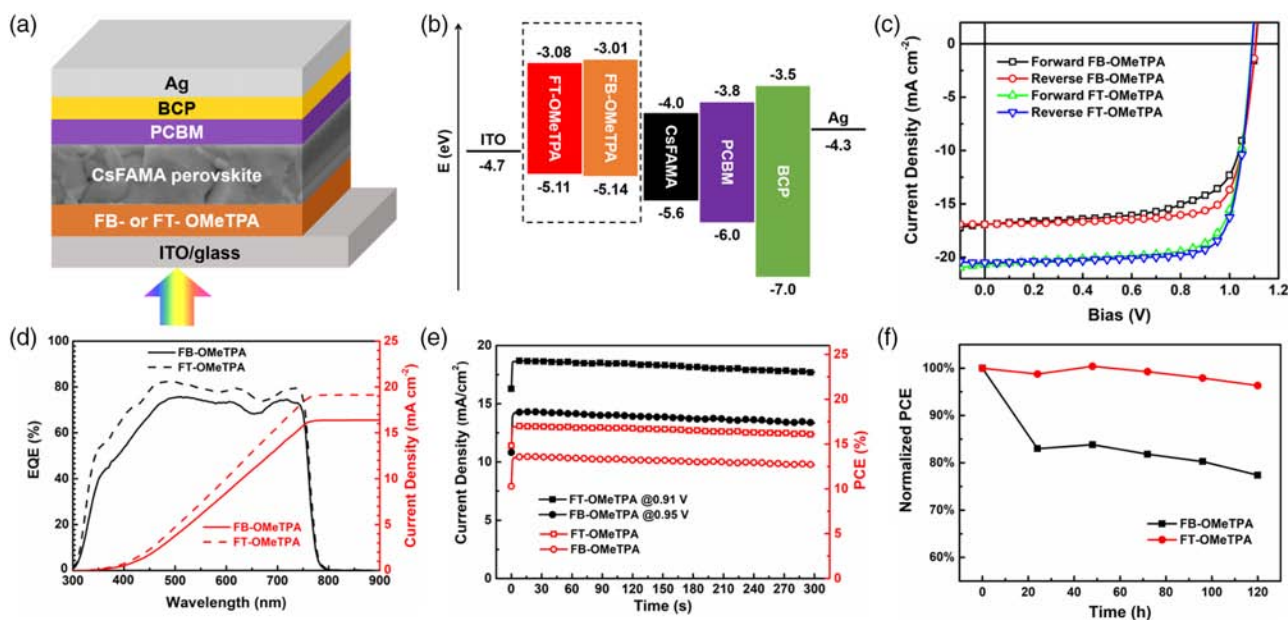


Figure 4. a) Device structure of the inverted PVSCs with FB-OMeTPA or FT-OMeTPA as HTLs. b) Scheme of energy levels of the materials involved in the inverted PVSCs, the energy level data of the materials are cited from the previous study^[28] except FB-OMeTPA and FT-OMeTPA. c) The J - V characteristics and d) EQE spectra of devices with FB-OMeTPA or FT-OMeTPA as HTLs. e) Stabilized photocurrent measurement of the PVSCs based on FB-OMeTPA and FT-OMeTPA as HTLs at maximum power point under 1 sun illumination. f) PCEs normalized to the maximum efficiencies of the devices based on FB-OMeTPA and FT-OMeTPA, respectively. The PVSCs were all stored in dark and dry air (20% RH) at room temperature without encapsulation.

Table 1. Device performances of PVSCs using FB-OMeTPA and FT-OMeTPA as HTLs under AM1.5G illumination with the intensity of 100 mW cm^{-2} .

HTL	Scan direction	V_{oc} [V]	FF [%]	J_{sc} [mA cm^{-2}]	PCE [%]	Average PCE ^a [%]	integrated J_{sc} [mA cm^{-2}]
FB-OMeTPA	Forward	1.11	68.87	16.93	12.90	12.58 0.47	16.37
	Reverse	1.11	76.75	16.91	14.35	13.66 0.57	
FT-OMeTPA	Forward	1.09	75.09	20.70	16.95	16.07 0.52	19.12
	Reverse	1.09	78.43	20.50	17.57	16.65 0.58	

^aAverage PCE including the standard errors. The statistics is based on ten cells on different substrates for each HTL.

Pb peak is observed, and the peak of S at 163.2 eV shifts about 0.1 eV to the left. The aforementioned results suggest the interaction between Pb^{2+} and S.^[29] Combining the theoretical calculation and XPS results, the passivation effect of FT-OMeTPA on perovskites can be validated, leading to an apparently suppressed hysteresis of the devices.

To compare the hole extraction ability of FB-OMeTPA and FT-OMeTPA as HTLs, charge collection probability (P_{cc}) of these two materials is investigated. P_{cc} with respect to internal voltage (V_{int}) under 100 mW cm^{-2} AM1.5G solar illumination is defined by Equation (1)–(3)^[28,37]

$$P_{cc} = J_{ph} / J_{ph, sat} \quad (1)$$

$$J_{ph} = J_L - J_D \quad (2)$$

$$V_{int} = V_{bi} - V_{appl} \quad (3)$$

where J_{ph} is the photocurrent density. $J_{ph, sat}$ is the saturated photocurrent density at reverse bias. J_L and J_D are the current density

with and without illumination, respectively. J_{ph} goes saturation with increasing V_{int} , so we choose J_{ph} at $V_{int} = 2.5 \text{ V}$ as $J_{ph, sat}$. V_{bi} is the built-in potential of the device referring to the voltage at $J_{ph} = 0$. V_{appl} is the applied bias. V_{bi} of 1.11 V is obtained for the FB-OMeTPA-based device, higher than that of the FT-OMeTPA based device (1.08 V). The higher V_{bi} for FB-OMeTPA based device can be attributed to the deeper HOMO level of FB-OMeTPA, which can facilitate the charge extraction. However, the space-charge-limited-current (SCLC) hole mobility of FT-OMeTPA ($1.42 \times 10^5 \text{ cm}^2 \text{ V}^{-1} \text{ s}^{-1}$) is higher than that of FB-OMeTPA ($3.61 \times 10^6 \text{ cm}^2 \text{ V}^{-1} \text{ s}^{-1}$), which is shown in Table S9, Supporting Information. In addition, the computational results demonstrate that S atoms in FT cores have stronger interactions with Pb^{2+} ions and passivate the traps at the perovskite/HTL interface. As a comprehensive result, a higher P_{cc} of 97.1% is achieved by the FT-OMeTPA-based device than 96.2% for the FB-OMeTPA-based device at short-circuit condition, which is shown in Figure S16, Supporting Information, implying better charge extraction ability of FT-OMeTPA.

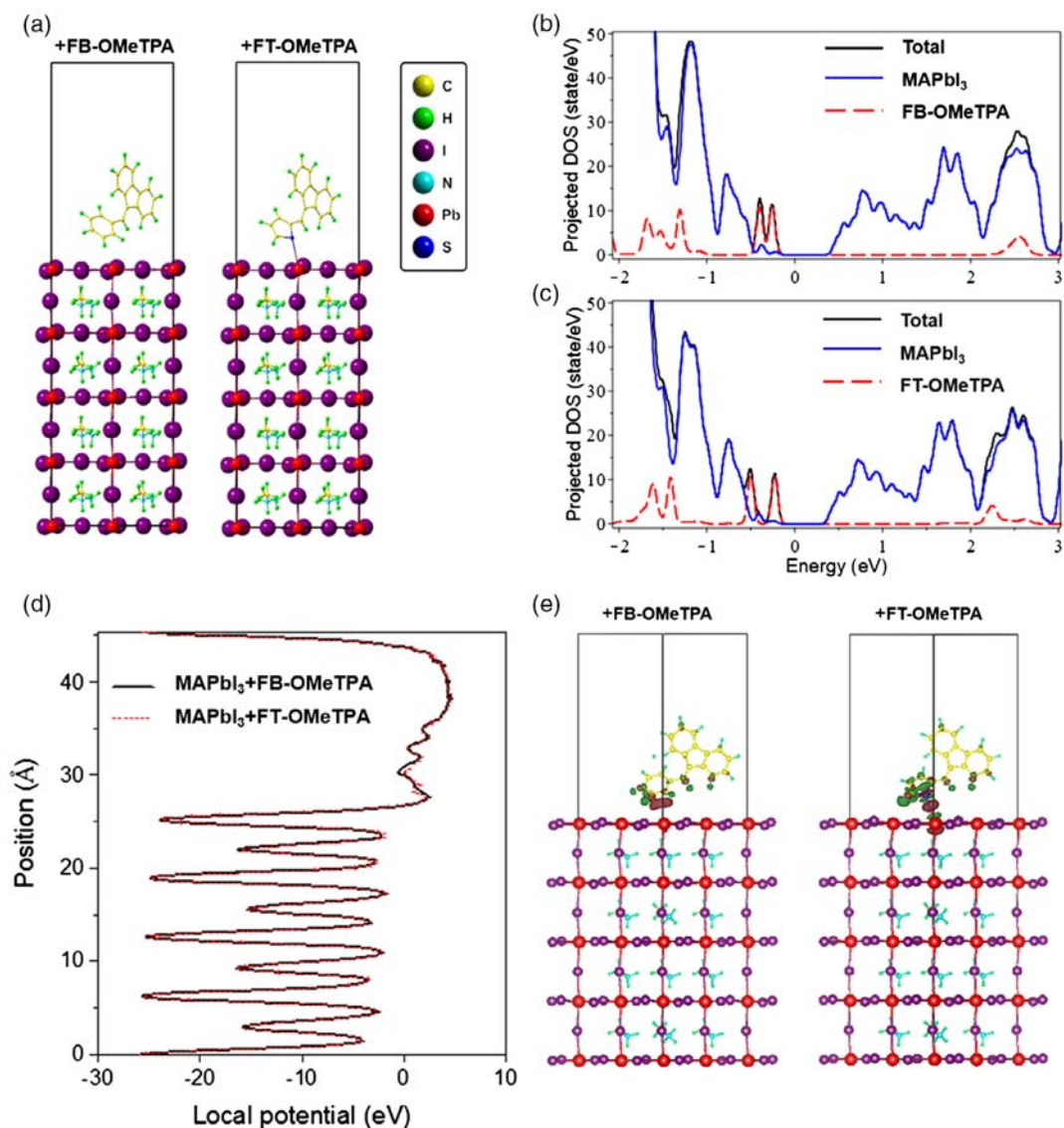


Figure 5. a) The stable structures viewed from *a* axis for the absorption of FB-OMeTPA molecule (the left one) and FT-OMeTPA molecule (the right one) onto (001)-surface of perovskites MAPbI₃. b,c) The total and projected DOS for the two structures in (a). d) The position-resolved total electrostatic potential along *c* axis for the two structures in (a). e) The charge density differences between the total system and the sum of the individual components (i.e., MAPbI₃ and FB/FT-OMeTPA molecule) for the two cases in (a). The green (brown) color represents negative (positive) charge density. The isosurface is chosen to be at the same value (around 15% of the maximum values).

To achieve greater understanding of the recombination kinetic in devices, J_{SC} and V_{OC} are measured by varying the incident light intensity (P_{light}) from 9 to 101 mW cm⁻². **Figure 6a** shows the log-log data of J_{SC} versus P_{light} , and J_{SC} qualitatively follows the power-law dependence, where $J_{SC} \propto P_{light}^\alpha$. The exponents (α) are close to unity for the devices based on both FB-OMeTPA and FT-OMeTPA, suggesting that the bimolecular recombination is suppressed at the interfaces between perovskite and transporting layers and almost all carriers are swept out prior to recombination at short-circuit condition.^[28,38] This is in good agreement with the discussion on P_{cc} . **Figure 6b** shows the logarithmic dependence of V_{OC} with incident light intensity ($\ln P_{light}$). The slopes for FB-OMeTPA- and FT-OMeTPA-based devices are

1.64 and 1.58 kT q⁻¹, respectively. Usually, the slopes greater than kT q⁻¹ indicate that Shockley-Read-Hall (SRH) recombination is involved. Smaller slope of FT-OMeTPA-based device implies less amount of SRH recombination at open circuit.^[39] The aforementioned results demonstrate that FT-OMeTPA can passivate the trap state at the interface between perovskite film and HTL, leading to reduced hysteresis.

Steady-state and time-resolved photoluminescence (PL) are also measured to investigate the ability of the HTLs to extract holes. As shown in **Figure 6c**, comparing with the PL spectra of neat perovskite film grown on glass, the PL intensity can be quenched by the introduction of ITO and HTLs, and most efficiently for FT-OMeTPA, implying the good hole extraction.

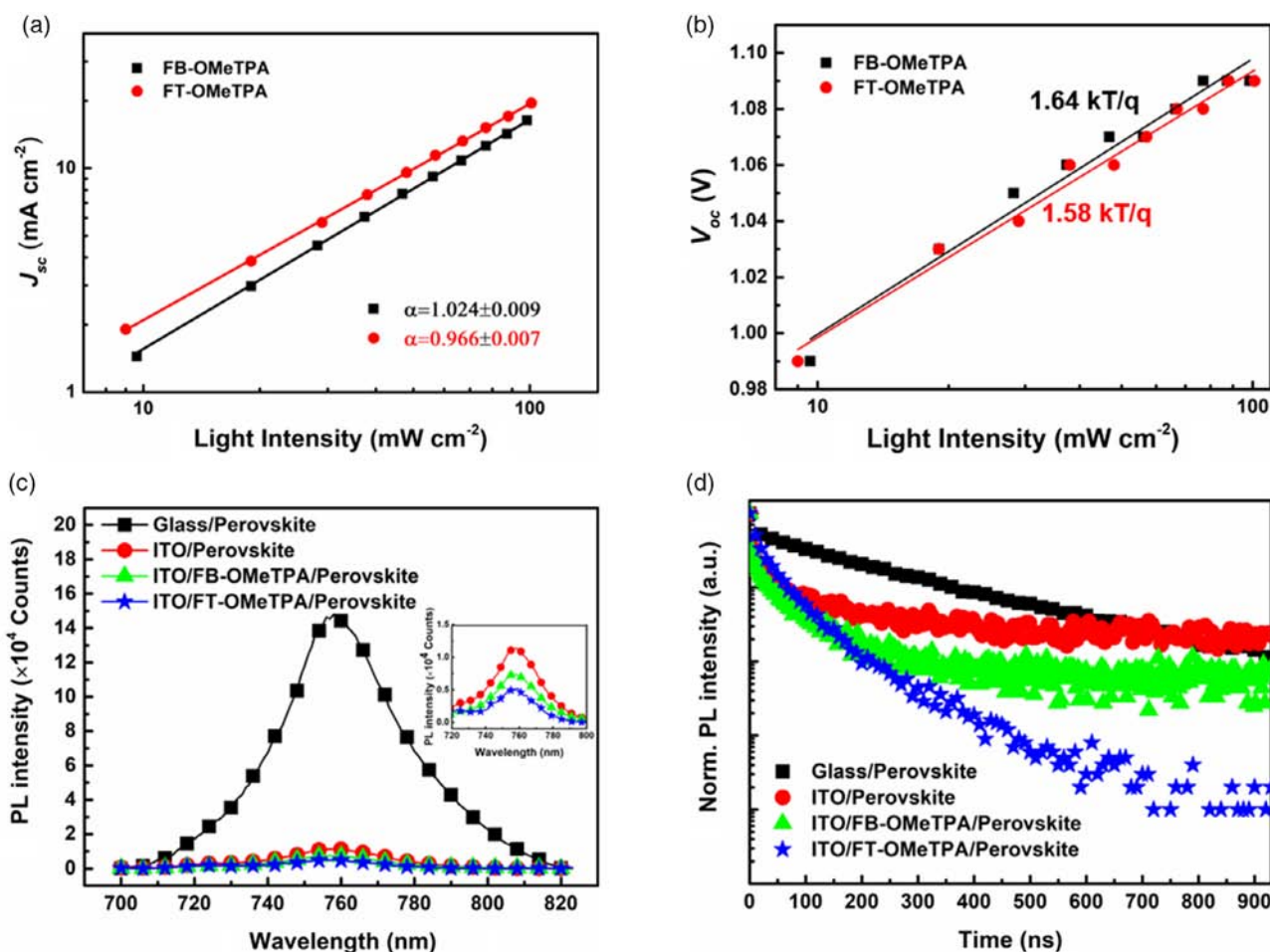


Figure 6. Light-intensity dependence of a) short-circuit current density (J_{sc}) and b) open-circuit voltage (V_{oc}) of the devices with FB-OMeTPA or FT-OMeTPA as HTLs. c) Steady-state PL spectra and d) time-resolved PL decay measurements of the perovskite films on different substrates (glass only, ITO, ITO/FB-OMeTPA, and ITO/FT-OMeTPA).

Figure 6d shows the results of time-resolved PL decay measurements, and all the curves are fitted by biexponential decay function (Table 2). Perovskite films grown on glass only and on ITO exhibit an average decay time (ave. τ) of 240.5 and 90.2 ns, respectively. There is an ave. τ of 70.2 ns for the perovskite/FB-OMeTPA/ITO structure. In the case of perovskite/FT-OMeTPA/ITO, it has the shortest ave. τ of 47.5 ns, indicating the efficient interfacial charge transfer from perovskite to FT-OMeTPA. The shorter ave. τ is also another evidence for better trap states passivation than FB-OMeTPA.

Table 2. Fitting results of time-resolved PL decay measurements.

Sample	τ_1 [ns]	frac. 1 [%]	τ_2 [ns]	frac. 2 [%]	ave. τ [ns]
Glass	91.6	17.03	271.1	82.97	240.5
ITO	10.7	21.15	98.6	78.85	90.2
FB ^{a)}	24.7	57.09	91.1	42.91	70.2
FT ^{b)}	12.7	33.95	65.4	66.06	47.5

^{a)}FB-OMeTPA; ^{b)}FT-OMeTPA.

In summary, two novel dopant-free HTMs with similar structure, namely, FB-OMeTPA and FT-OMeTPA, are developed for inverted PVSCs. Between the two facile synthesized molecules, FT-OMeTPA possesses a much higher hole mobility than FB-OMeTPA by the introduction of thiophene unit. Our results clearly reveal the strong Pb^{2+} -S interaction at the interface of FT-OMeTPA/perovskite, which is beneficial for passivating the defects at the surface of perovskite, leading to the suppressed recombination of carriers and hysteresis. The good hole extraction ability and cost of only \$28/g enable FT-OMeTPA a promising candidate as HTM for efficient low-cost PVSCs.

Supporting Information

Supporting Information is available from the Wiley Online Library or from the author.

Acknowledgements

F.M. and Y.J. contributed equally to this work. This research was funded by the Leading Talents of Guangdong Province Program (2016LJ06N507),

Shenzhen Basic Research Fund (CY20170817110652558), the National Key Research and Development Program of China (2018YFB0704100), the Key Areas Research and Development Program of Guangdong Province (2019B010941001), Shenzhen Basic Research Fund under Grant No. JCY20170817105201098, the Natural Science Foundation of China (Grant Nos. 51603086 and 21576112), the Natural Science Foundation Project of Jilin Province (Grant Nos. 20160520131JH, 20180101181JC, and 20180623042TC), the Project of Human Resources and Social Security Department of Jilin Province (2017956), the Project of Jilin Province Development and Reform Commission (2019C044), and the Science and Technology Research Project of the Department of Education of Jilin Province (2016-218). The computational resource was supported by Center for Computational Science and Engineering of Southern University of Science and Technology.

Conflict of Interest

The authors declare no conflict of interest.

Keywords

dopant-free, hole transporting materials, interfacial interactions, inverted perovskite photovoltaics, p-i-n

Received: July 18, 2019

Revised: September 5, 2019

Published online: September 19, 2019

- [1] A. Kojima, K. Teshima, Y. Shirai, T. Miyasaka, *J. Am. Chem. Soc.* **2009**, *131*, 6050.
- [2] NREL, <https://www.nrel.gov/pv/cell-efficiency.html> (accessed: August 2019).
- [3] A. Rajagopal, K. Yao, K.-Y. Jen Alex, *Adv. Mater.* **2018**, *30*, 1800455.
- [4] A. Polman, M. Knight, E. C. Garnett, B. Ehrler, W. C. Sinke, *Science* **2016**, *352*, aad4424.
- [5] W. S. Yang, J. H. Noh, N. J. Jeon, Y. C. Kim, S. Ryu, J. Seo, S. I. Seok, *Science* **2015**, *348*, 1234.
- [6] A. D. Jodlowski, C. Roldán-Carmona, G. Grancini, M. Salado, M. Ralaifarisoa, S. Ahmad, N. Koch, L. Camacho, G. de Miguel, M. K. Nazeeruddin, *Nat. Energy* **2017**, *2*, 972.
- [7] T. Bu, J. Li, F. Zheng, W. Chen, X. Wen, Z. Ku, Y. Peng, J. Zhong, Y. B. Cheng, F. Huang, *Nat. Commun.* **2018**, *9*, 4609.
- [8] D. Bi, C. Yi, J. Luo, J. D. Décoppet, F. Zhang, S. M. Zakeeruddin, X. Li, A. Hagfeldt, M. Grätzel, *Nat. Energy* **2016**, *1*, 16142.
- [9] Q. Jiang, L. Zhang, H. Wang, X. Yang, J. Meng, H. Liu, Z. Yin, J. Wu, X. Zhang, J. You, *Nat. Energy* **2016**, *2*, 16177.
- [10] A. Abate, T. Leijtens, S. Pathak, J. Teuscher, R. Avolio, M. E. Errico, J. Kirkpatrick, J. M. Ball, P. Docampo, I. McPherson, H. J. Snaith, *Phys. Chem. Chem. Phys.* **2013**, *15*, 2572.
- [11] Y. Wang, Z. Zhu, C. C. Chueh, A. K.-Y. Jen, Y. Chi, *Adv. Energy Mater.* **2017**, *7*, 1700823.
- [12] Z. H. Bakr, Q. Wali, A. Fakharuddin, L. Schmidt-Mende, T. M. Brown, R. Jose, *Nano Energy* **2017**, *34*, 271.
- [13] J. Liu, Y. Wu, C. Qin, X. Yang, T. Yasuda, A. Islam, K. Zhang, W. Peng, W. Chen, L. Han, *Energy Environ. Sci.* **2014**, *7*, 2963.
- [14] F. Zhang, C. Yi, P. Wei, X. Bi, J. Luo, G. Jacopin, S. Wang, X. Li, Y. Xiao, S. M. Zakeeruddin, M. Grätzel, *Adv. Energy Mater.* **2016**, *6*, 1600401.
- [15] S. Paek, P. Qin, Y. Lee, K. T. Cho, P. Gao, G. Grancini, E. Oveisi, P. Gratia, K. Rakstys, S. A. Al-Muhtaseb, C. Ludwig, J. Ko, M. K. Nazeeruddin, *Adv. Mater.* **2017**, *29*, 1606555.
- [16] M. Stolterfoht, C. M. Wolff, Y. Amir, A. Paulke, L. Perdígón-Toro, P. Caprioglio, D. Neher, *Energy Environ. Sci.* **2017**, *10*, 1530.
- [17] Y. Feng, Q. Hu, E. Rezaee, M. Li, Z.-X. Xu, A. Lorenzoni, F. Mercuri, M. Muccini, *Adv. Energy Mater.* **2019**, *9*, 1901019.
- [18] L. Zhang, C. Liu, X. Wang, Y. Tian, A. K. Y. Jen, B. Xu, *Adv. Funct. Mater.* **2019**, 1904856, <https://doi.org/10.1002/adfm.201904856>.
- [19] Y. Wang, W. Chen, L. Wang, B. Tu, T. Chen, B. Liu, K. Yang, C. W. Koh, X. Zhang, H. Sun, G. Chen, X. Feng, H. Y. Woo, A. B. Djurišić, Z. He, X. Guo, *Adv. Mater.* **2019**, *31*, 1902781.
- [20] Z. Zhu, Y. Bai, T. Zhang, Z. Liu, X. Long, Z. Wei, Z. Wang, L. Zhang, J. Wang, F. Yan, S. Yang, *Angew. Chem.* **2014**, *126*, 12779.
- [21] J. B. You, L. Meng, T. B. Song, T. F. Guo, Y. Yang, W. H. Chang, Z. R. Hong, H. J. Chen, H. P. Zhou, Q. Chen, Y. S. Liu, N. De Marco, Y. Yang, *Nat. Nanotechnol.* **2016**, *11*, 75.
- [22] Z. Y. Liu, J. J. Chang, Z. H. Lin, L. Zhou, Z. Yang, D. Z. Chen, C. F. Zhang, S. Z. Liu, Y. Hao, *Adv. Energy Mater.* **2018**, *8*, 9.
- [23] C. Zuo, L. Ding, *Adv. Energy Mater.* **2017**, *7*, 1601193.
- [24] C. Li, Q. Guo, Z. Wang, Y. Bai, L. Liu, F. Wang, E. Zhou, T. Hayat, A. Alsaedi, Z. Tan, *ACS Appl. Mater. Interfaces* **2017**, *9*, 41937.
- [25] W. Q. Zhou, Z. H. Wen, P. Gao, *Adv. Energy Mater.* **2018**, *8*, 1702512.
- [26] E. Rezaee, X. Liu, Q. Hu, L. Dong, Q. Chen, J.-H. Pan, Z.-X. Xu, *Sol. RRL* **2018**, *2*, 1800200.
- [27] X. Liu, X. Zheng, Y. Wang, Z. Chen, F. Yao, Q. Zhang, G. Fang, Z.-K. Chen, W. Huang, Z.-X. Xu, *ChemSusChem* **2017**, *10*, 2833.
- [28] H. Chen, W. Fu, C. Huang, Z. Zhang, S. Li, F. Ding, M. Shi, C.-Z. Li, A. K.-Y. Jen, H. Chen, *Adv. Energy Mater.* **2017**, *7*, 1700012.
- [29] X. Lai, F. Meng, Q.-Q. Zhang, K. Wang, G. Li, Y. Wen, H. Ma, W. Li, X. Li, A. K. K. Kyaw, K. Wang, X. W. Sun, M. Du, X. Guo, J. Wang, W. Huang, *Sol. RRL* **2019**, *3*, 1900011.
- [30] T. Malinauskas, M. Saliba, T. Matsui, M. Daskeviciene, S. Urnikaite, P. Gratia, R. Send, H. Wonneberger, I. Bruder, M. Grätzel, V. Getautis, M. K. Nazeeruddin, *Energy Environ. Sci.* **2016**, *9*, 1681.
- [31] F. Zhang, Z. Wang, H. Zhu, N. Pellet, J. Luo, C. Yi, X. Liu, H. Liu, S. Wang, X. Li, Y. Xiao, S. M. Zakeeruddin, D. Bi, M. Grätzel, *Nano Energy* **2017**, *41*, 469.
- [32] C. Huang, W. Fu, C.-Z. Li, Z. Zhang, W. Qiu, M. Shi, P. Heremans, A. K. Y. Jen, H. Chen, *J. Am. Chem. Soc.* **2016**, *138*, 2528.
- [33] K. M. M. Salim, T. M. Koh, D. Bahulayan, P. C. Harikesh, N. F. Jamaludin, B. Febriansyah, A. Bruno, S. Mhaisalkar, N. Mathews, *ACS Energy Lett.* **2018**, *3*, 1068.
- [34] P. Hohenberg, W. Kohn, *Phys. Rev.* **1964**, *136*, B864.
- [35] W. Kohn, L. J. Sham, *Phys. Rev.* **1965**, *140*, A1133.
- [36] I. Garcia-Benito, I. Zimmermann, J. Urieta-Mora, J. Aragón, J. Calbo, J. Perles, A. Serrano, A. Molina-Ontoria, E. Ortí, N. Martín, M. K. Nazeeruddin, *Adv. Funct. Mater.* **2018**, *28*, 1801734.
- [37] A. K. K. Kyaw, D. H. Wang, D. Wynands, J. Zhang, T.-Q. Nguyen, G. C. Bazan, A. J. Heeger, *Nano Lett.* **2013**, *13*, 3796.
- [38] R. Azmi, S.-H. Oh, S.-Y. Jang, *ACS Energy Lett.* **2016**, *1*, 100.
- [39] S. R. Cowan, A. Roy, A. J. Heeger, *Phys. Rev. B* **2010**, *82*, 245207.